

Extreme outbreak dynamics in epidemic models

Jason Hindes¹, Michael Assaf^{2,3}, and Ira B. Schwartz¹

¹*U.S. Naval Research Laboratory, Washington, DC 20375, USA*

²*Racah Institute of Physics, Hebrew University of Jerusalem, Jerusalem 91904, Israel and*

³*Institute for Physics and Astronomy, University of Potsdam, Potsdam 14476, Germany*

The COVID-19 pandemic has demonstrated how disruptive emergent disease outbreaks can be and how useful epidemic models are for quantifying risks of local outbreaks. Here we develop an analytical approach to calculate the dynamics and likelihood of outbreaks within the canonical Susceptible-Exposed-Infected-Recovered and more general models, including COVID-19 models, with fixed population sizes. We compute the distribution of outbreak sizes including extreme events, and show that each outbreak entails a unique, depletion or boost in the pool of susceptibles and an increase or decrease in the effective recovery rate compared to the mean-field dynamics— due to finite-size noise. Unlike extreme events occurring in long-lived metastable stochastic systems, the underlying outbreak distribution depends on a full continuum of optimal paths, each connecting two unique non-trivial fixed-points, and thus represents a novel class of extreme dynamics.

Introduction. Epidemic models are useful for predicting the dynamics of infectious diseases, rumors, election outcomes, fads, and computer viruses[1–8]. In particular in the early days of emerging disease outbreaks, such as the current COVID-19 pandemic, societies rely on predictive models to identify the most effective control strategies for minimizing infectious contacts within a population[9–12]. To this end it is useful to quantify the risks of local outbreaks of various sizes. Within a given population, outbreak dynamics are typically described in terms of compartmental models[1, 4, 13]. For example, starting from some seed infection, over time individuals in a population make transitions between some number of discrete disease states (susceptible, exposed, infectious, etc.) based on prescribed probabilities for a particular disease[9, 10, 12, 14–16]. In the limit of infinite populations the stochastic dynamics approach deterministic (mean-field) differential equations for the expected fraction of a population in each state[1, 4, 13, 17].

Yet, for real finite populations outbreak dynamics have a wide range of different outcomes for each initial condition. A natural question is, what is the distribution of outbreak sizes? Beside stochastic simulations[1, 14, 17, 18], methods exist for e.g., recursively calculating the full outbreak statistics[16, 19, 20], solving the master equation for the underlying stochastic dynamics directly by numerical linear algebra[18], or deriving scaling laws for small outbreaks near threshold[21–23]. However, in addition to being numerically unstable for large populations, computationally expensive, or limited in scope, such methods also fail to provide physical and analytical insights into how unusual and extreme outbreaks occur.

Here we develop an analytical approach based on WKB-methods[24–26] which provides a closed-form expression for the asymptotic outbreak distribution in canonical SIR, SEIR, and COVID-19 models with fixed population sizes (N) and heterogeneity in infectivity and recovery[12, 27–29]. We show that each extreme outbreak is described by a unique, most-probable path. Compared to the expected mean-field solution each outbreak entails a unique, depletion or boost in the pool of suscepti-

bles and an increase or decrease in the effective recovery rate compared to the mean-field dynamics, depending on whether the outbreak is larger or smaller than the expected value. Moreover, unlike usual rare-event predictions for epidemic dynamics, such as extinction or other large fluctuations from an endemic state[26, 30–32], and fade-out[33], our results do not rely on the existence of a metastable state [25, 34–37], and thus are valid for the comparatively short time scales of outbreaks, $\mathcal{O}(\ln N)$ [38]. Finally, and in sharp contrast to systems undergoing escape from a metastable state, we show that the extreme outbreak distribution corresponds to an infinite number of distinct paths— one for every possible final outbreak. Each path connects two fixed-points, at the beginning and end of an outbreak, *both* with non-zero probability flux. In this way extreme outbreaks represent a distinct class of rare events for discrete-state systems.

Outbreak model. We begin with the Susceptible-Infected-Recovered (SIR) model, often used as a baseline model for disease outbreaks[1, 2, 4, 13]. Individuals are either susceptible (capable of getting infected), infected, or recovered/deceased. Denoting the total number of susceptibles S , infecteds I , and recovereds R in a population of fixed size N , the probability per unit time that the number of susceptibles decreases by one and the number of infecteds increases by one is $\beta SI/N$, where β is the infectious contact rate[1, 2, 4]. Similarly, the probability per unit time that the number of infecteds decreases by one is γI , where γ is the recovery rate[1, 2, 4]. As N is assumed constant, the model is appropriate for the short time scales of early emergent-disease outbreaks, with an assumed separation between the outbreak dynamics and demographic time scales, as well as re-infection[1]. From the basic reactions, the master equation describing the full probability of states at time t is

$$\begin{aligned} \frac{\partial P}{\partial t}(S, I, t) = & -\frac{\beta SI}{N}P(S, I, t) - \gamma IP(S, I, t) + \\ & \frac{\beta(S+1)(I-1)}{N}P(S+1, I-1, t) + \gamma S(I+1)P(S, I+1, t). \end{aligned} \quad (1)$$

In general such equations cannot be solved analytically.

ically, and one must resort to high-dimensional numerics, recursive calculations, and/or large numbers of simulations[18]. Yet, if N is large it is possible to construct an asymptotic solution to Eq.(1) for all $\mathcal{O}(N)$ outbreaks using WKB methods[24–26], as we will show.

Let us define the fraction of individuals in each disease state $x_w = W/N$ where $W \in \{S, I, R\}$. Note that since the total population size is constant, $x_r = 1 - x_s - x_i$. For large but finite N we assume a WKB form for the probability, $P(x_s, x_i) \simeq A(x_s, x_i) \exp\{-N\mathcal{S}(x_s, x_i)\}$, which is the general scaling form for large deviations in population models with a small $\mathcal{O}(1/N)$ noise parameter [24–26, 30]. Direct numerical evidence also suggests the WKB form—see Fig.1, where the fraction of 10^{11} simulations that result in 100% (blue), 98% (red), and 96% (green) of a population infected are plotted versus N (note: the mean-field outbreak size is 89%). Simulations were performed using Gillespie’s direct method[1, 14, 39] starting from a single infectious individual. Indeed, we can see that the log of the probability scales linearly with N . The slopes of the lines in Fig.1 are predicted from our WKB theory.

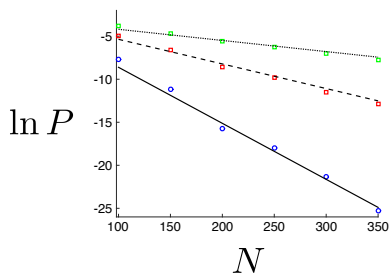


FIG. 1. Extreme outbreak probability scaling with the population size in the SIR model. Plotted is the probability that 100% (blue), 98% (red), and 96% (green) of the population are infected during an outbreak versus the population size. Points denote simulation results. The slopes of the lines are equal to the predicted actions from Eq.(7). Here $R_0=2.5$.

Substituting the WKB ansatz into Eq.(1), and keeping leading-order terms in $N \gg 1$, we arrive at a Hamilton-Jacobi equation, $\partial_t \mathcal{S}(x_s, x_i) + H(x_s, x_i, p_s, p_i) = 0$, with $p_w = \partial_{x_w} \mathcal{S}$ [24, 25] and where the Hamiltonian is

$$H = \beta x_i x_s (\exp\{p_i - p_s\} - 1) + \gamma x_i (\exp\{-p_i\} - 1). \quad (2)$$

As a consequence for large N , the outbreak dynamics satisfy Hamilton’s equations[24, 25], $\dot{x}_w = \partial_{p_w} H$ and $\dot{p}_w = -\partial_{x_w} H$ given Eq.(2), just as in analytical mechanics[40]. Once Hamilton’s equations are solved, the probability exponent $\mathcal{S}(x_s, x_i)$, called the action, can be calculated along an outbreak: $\mathcal{S}(x_s, x_i) = \int p_s dx_s + \int p_i dx_i - \int H dt$.

Before continuing our analysis, let us comment on the outbreak distribution, $P(x_s, x_i)$, and explain the sense in which certain outbreaks are extreme. Since $P(x_s, x_i)$ scales exponentially with N (for large N), if the action $\mathcal{S}(x_s, x_i)$ associated with an outbreak differs significantly from 0, the outbreak will occur with an exponentially

small probability. In general the deterministic (mean-field) SIR model solution corresponds to an $\mathcal{S} = 0$ solution, and it implies a certain final outbreak, $x_r^0(t \rightarrow \infty)$ with a known formula[1, 41]. But, what about a half, a fourth, twice, etc. of this expected outbreak, or a case in which the entire population eventually becomes infected? Even though such outbreaks with $\mathcal{S} > 0$ are unusual and unlikely, we would like to know what their probabilities are and how they occur. Another useful implication of the WKB approach is that since the action satisfies a Hamilton-Jacobi equation, the outbreak paths are minimum-action[25], or maximum-probability solutions. Namely, given boundary conditions for an outbreak, the WKB solution will provide the most-likely dynamics.

Results. To find the paths and probabilities for extreme outbreaks, first, we go back to Eq.(2). Since the Hamiltonian does not depend explicitly on time, H evaluated along an outbreak is conserved in time[40]. Given Eq.(2), it is easy to show that for the SIR model $H = -x_i \dot{p}_i$. As we are interested in outbreak dynamics that start from small infection, e.g., $x_i(t=0) = 1/N$ with $N \gg 1$, for such outbreaks $H \approx 0$. Of course $x_i(t) \neq 0$ during the course of such outbreaks—since infection grows over time—and thus it must be that $p_i = \text{const}$ in general.

Let us define two useful constants: $m \equiv \exp\{p_i\}$ and the standard reproductive number $R_0 \equiv \beta/\gamma$ [1, 2, 4, 13]. Since $\dot{p}_i = 0$, the fluctuational momentum p_s along an outbreak is known in terms of x_s , m , and R_0 :

$$\exp\{p_s\} = R_0 x_s m^2 / [m(R_0 x_s + 1) - 1]. \quad (3)$$

In general, Eq.(3) implies that the momentum p_s is non-zero during an extreme outbreak; for instance, $p_s \neq 0$ at the initial condition $x_s(t=0) = 1$. The same is true near the final state, $x_s^* = x_s(t \rightarrow \infty)$, which determines the total outbreak size, $x_r^*(m) = 1 - x_s^*(m)$, or the total fraction of the population infected over all times.

The next important step is to find $x_s^*(m)$. First, we use the fact that $\sum_w \dot{x}_w = 0$, since the total population is constant, which gives us $\dot{x}_r = (\gamma/m)x_i$. Second, evaluating dx_s/dx_r , results in a differential equation that can be solved for x_s^* , $dx_s/dx_r = -R_0 x_s m^2 \exp\{-p_s\}$. Integrating x_s from 1 to x_s^* , and x_r from 0 to $1 - x_s^*$, yields a single implicit equation for the final outbreak versus m :

$$\exp[R_0 m(1 - x_s^*)] = [m(R_0 + 1) - 1] / [m(R_0 x_s^* + 1) - 1]. \quad (4)$$

Thus, for fixed R_0 , we have a complete mapping between the final outbreaks and the free-parameter m : each outbreak corresponds to a unique value of m ; given x_s^* , it is easy to check that the final momentum, p_s^* , is also non-zero from Eq.(3). Solving Eq. (4) for m , we find

$$x_s^* = \left\{ 1 - m - W_0 \left[(1 - m(R_0 - 1)) e^{1 - m(R_0 + 1)} \right] \right\} / (m R_0), \quad (5)$$

where $W_0(z)$ is the principle solution for w of $z = w e^w$.

We can also find the trajectory for the population frac-

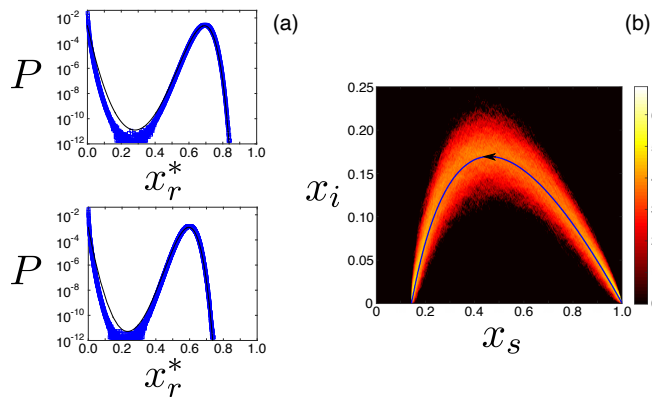


FIG. 2. Extreme outbreak distributions. (a) Final outbreak distribution for the SIR model (top) and a COVID-19 model (bottom). Stochastic simulation results are shown with blue squares and theory predictions with black lines. Parameters are $N=2000$ and $R_0=1.7$ for the top, and $N=4000$, $\beta_1=1.8$, $\beta_2=1.12$, $\gamma_1=1$, $\gamma_2=0.8$, $\alpha=2$, and $z_1=0.3$ for the bottom. (b) Heat map showing the log-density of stochastic simulation trajectories that result in $x_r^* N=856$; the mean-field outbreak is $x_r^* N=691$. The predicted trajectory, Eq.(6), is shown with a blue curve. Parameters are $N=1000$ and $R_0=1.7$.

tion infected during an outbreak by solving dx_i/dx_s ,

$$x_i(x_s, m) = 1 - x_s + \ln \left[\frac{m(R_0 x_s + 1) - 1}{m(R_0 + 1) - 1} \right] / R_0 m. \quad (6)$$

Having found $p_s(x_s)$ and the total outbreak, $x_r^* = 1 - x_s^*$, we can perform the integral $\int p_s dx_s$ for the action:

$$\begin{aligned} \mathcal{S}(m, x_s^*(m)) &= \ln x_s^* + (1 - x_s^*) \\ &\times [m(1 + R_0 x_s^*) - 1 + \ln [(m(R_0 + 1) - 1)/(x_s^{*m} m^2 R_0)]] . \end{aligned} \quad (7)$$

Note that $\int p_i dx_i = 0$, as p_i is constant and $x_i = 0$ at both boundaries. By combining Eq.(4) and Eq.(7) we have a one-parameter (m) family of total outbreaks and their associated probabilities – on log scale – which represents a complete asymptotic analytical solution for the extreme $\mathcal{O}(N)$ outbreak distribution when N is large but finite.

Comparisons between Eqs.(4-7) and stochastic simulations of the SIR model are shown in Fig.2 (a). The fraction of 10^{12} simulations that resulted in an outbreak x_r^* are plotted in blue, and the solutions of Eqs.(4-7) with a black line. The agreement between the two is quite good for the population size $N=2000$ and $R_0=1.7$. Disagreement increases as the outbreak number approaches $\mathcal{O}(1)$. Nevertheless, the accuracy of the WKB becomes asymptotically exact as $N \rightarrow \infty$ [24, 30]. Qualitatively, the distribution has a cubic structure with local maxima at the smallest outbreak (here $1/N$) and the mean-field solution[24, 30, 33, 35]. In between is a minimum (near $x_r^* \approx 0.28$ in Fig.2 (a)) that we call the least-likely small outbreak, x_r^m , $\partial \mathcal{S} / \partial x_s^*(x_r^m) = 0$ from (7). For outbreaks smaller than the mean field, x_r^m can be used to separate outbreaks into increasing or decreasing likelihoods.

Further exploring our solution, we show an example of what stochastic trajectories look like that result in an outbreak larger than the mean-field value in Fig.2 (b). Shown is a heat map built from 2000 stochastic simulations that have a final outbreak of 856 individuals. Note that the color map for trajectory-densities is on log scale. Also plotted is the predicted trajectory from Eq.(6), which lies in the yellow region with the highest density – demonstrating that, not only does our approach predict the extreme outbreak probabilities, but also the optimal dynamics that leads to such outbreaks.

In terms of analytical scaling, in Eq. (5) we have expressed x_s^* as a function of m which allows finding an explicit solution for the outbreak distribution as a function of x_s^* . While this gives rise to a highly cumbersome expression, further analytical progress can be done in the vicinity of $m \simeq 1$ – the maximum of the distribution. Expanding the right hand side of Eq. (5) around $m = 1$, we find m in terms of x_s^* : $m \simeq 1 - R_0(1 - R_0 x_0)(x_s^* - x_0)/[(1 - x_0)(1 + R_0^2 x_0)]$, with $x_0 \equiv -W_0(-R_0 e^{-R_0})/R_0$ being the mean-field solution of the final outbreak size. Indeed, m is close to 1 in the vicinity of the maximum of the distribution, $x_s^* \simeq x_0$. Plugging this expression into the action function (7), and approximating up to second order in $x_s^* - x_0$, we find $\mathcal{S}(x_s^*) \simeq (1/2)\mathcal{S}''(x_0)(x_s^* - x_0)^2$, with $\mathcal{S}''(x_0) = (R_0 x_0 - 1)^2 / [(1 - x_0)x_0(R_0^2 x_0 + 1)]$. This means that the distribution in the vicinity of x_0 is a Gaussian with a width of $\sigma = (N\mathcal{S}''(x_0))^{-1/2}$. Notably, close to the bifurcation, $R_0 - 1 \ll 1$, $x_0 \simeq 1 - 2(R_0 - 1)$, and the width simplifies to $\sigma \simeq 2/\sqrt{N(R_0 - 1)}$, whereas for $R_0 \gg 1$, $x_0 \simeq e^{-R_0}$ and $\sigma \simeq N^{-1/2}e^{-R_0/2}$. These calculations lead to a very interesting result: the coefficient of variation (COV), $COV = \sigma/x_0$, receives a minimum at $R_0 = 1.66$. That is, the deviation from the mean-field outbreak size is minimized at $R_0 \simeq 5/3$, whereas at $R_0 \rightarrow 1$ or $R_0 \gg 1$, the COV diverges, see Fig. 3 (a).

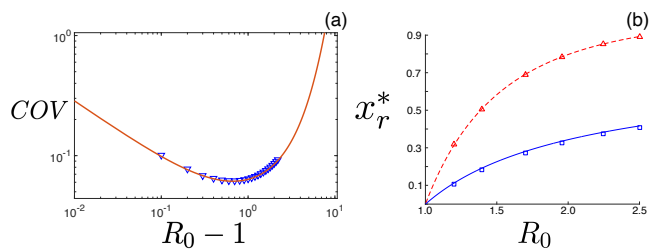


FIG. 3. Characteristics of the outbreak distribution. (a) Ratio of the distribution standard deviation (around the mean field) to its mean vs. $R_0 - 1$ on a log-log scale. Symbols are numerical solutions with Eq.(7) and $N = 5000$, while the line is given by σ/x_0 for the SIR model. (b) The least-likely (blue line) and most-likely (red line) outbreaks in the SEIR model versus $R_0 = \beta/\gamma$, computed from Eq. (7). Squares and triangles represent measured distribution minima and maxima from stochastic simulations. Population sizes are chosen so that $N\mathcal{S}(x_r^m)=17$. Other parameters are $\gamma=1$ and $\alpha=2$.

Before moving on to more general outbreak models we linger over a few important qualitative details of the ex-

treme outbreak dynamics that emerge from our analytical approach. In particular, let us consider the stochastic dynamics for the fraction of the population infected,

$$\dot{x}_i = \beta x_i \left[(m-1)/(mR_0) + x_s \right] - (\gamma/m)x_i. \quad (8)$$

First, note that when $m = 1$ ($p_i = p_s = 0$), we uncover the deterministic mean-field SIR model system, $\dot{x}_i = \beta x_i x_s - \gamma x_i$. From the latter, we can recover the more general Eq.(8) with the suggestive transformations $x_s \rightarrow x_s + (m-1)/mR_0$, and $\gamma \rightarrow \gamma/m$ [42]. Recalling that each extreme outbreak is parameterized by a constant m , evidently the effect of stochasticity in the finite- N SIR model is to add an effective constant reduction (or boost) to the pool of susceptibles and to increase (or decrease) the effective recovery rate, depending on whether the outbreak is smaller ($m < 1$) or larger ($m > 1$) than the mean-field solution, respectively.

Heterogeneous COVID-19 model. Now we turn to more complex models that derive from the basic SIR assumptions, but have more disease states and free parameters. In particular, epidemiological predictions for COVID-19 require an incubation period of around 5 days, and an asymptomatic disease state, i.e., a group of people capable of spreading the disease without documented symptoms[27–29]. Many models have been proposed to incorporate the spectrum of COVID-19 symptoms[9, 10, 12, 27–29]. A common assumption in such models is that upon infection, susceptible individuals first become exposed (E), and then enter an infectious state at a finite rate α . By assumption there are several possible infectious states (e.g., asymptomatic, mild, severe, etc.) that an exposed individual can enter according to prescribed probabilities [28, 29]. In addition, infectious states can have their own characteristic infection rates and recovery times. Following this approach, we define \mathcal{N} infectious states, I_n , where $n \in \{1, 2, \dots, \mathcal{N}\}$, each with their own infectious contact rate β_n and recovery rate γ_n , and which appear from the exposed state with probabilities z_n [12, 27–29, 43]. See SM for compact list of reactions.

Following the WKB-prescription above, the Hamiltonian for this general class of COVID-19 models is

$$H = \sum_n \beta_n x_{i,n} x_s (\exp\{p_e - p_s\} - 1) + \alpha z_n x_e (\exp\{p_{i,n} - p_e\} - 1) + \gamma_n x_{i,n} (\exp\{-p_{i,n}\} - 1). \quad (9)$$

To solve the system Eq.(9), let us adopt the convenient notation, $m = \exp\{p_e\}$, $m_s = \exp\{p_s\}$, and $m_{i,n} = \exp\{p_{i,n}\}$. As before, we look for solutions with $\dot{m}_{i,n} = 0$, or $\gamma_n(1 - 1/m_{i,n})/\beta_n = x_s(m/m_s - 1)$. Because the right hand side is a constant and the left hand side has no explicit dependence on (β_n, γ_n) , we define an outbreak *constant* $C(m) \equiv x_s(m/m_s - 1)$. Second, because $H = -x_e \dot{p}_e - \sum_n x_{i,n} \dot{p}_{i,n} = 0$, we have that $\dot{m} = 0$, or $m = \sum_n z_n m_{i,n}$. Altogether then, $C(m)$ is a solution of

$$m = \sum_n z_n / [1 - C(m)\beta_n/\gamma_n]. \quad (10)$$

Using $C(m)$ the action is given by a solvable integral $\mathcal{S}(m, x_s^*(m, C(m))) = \int_1^{x_s^*} \ln\{m x_s / (x_s + C(m))\} dx_s$. See SM for full equations and derivation of $x_s^*(m, C(m))$. An example of our general extreme-outbreak analysis is shown in the lower panel of Fig.2 (a). The analytical solution (black line) is in very good agreement with a COVID-19 model stochastic simulation with $N = 4000$, taking realistic, heterogeneous parameter values with an asymptomatic disease state[12, 27–29, 43].

Another interesting result of our analysis is that, in the special case of the SEIR model[1], where there is only one infectious state, the outbreak action is identical to the SIR model, Eq.(7). Namely, finite incubation changes the dynamics of extreme outbreaks, but has only a sub-exponential contribution to their probability. To test the result, in Fig.3 (b) we plot the predicted least-likely outbreak versus R_0 , where the predicted value (blue line) is compared with simulations (blue squares). The latter were determined by first building histograms from 10^{11} stochastic simulations in the SEIR model, similar to Fig.2 (a), and then fitting the smallest-probability region below the mean-field value. After fitting, the local minimum was extracted for each plotted value of R_0 . Here again, we find excellent agreement with our analytical formula.

Conclusions. In this letter we developed an analytical approach for predicting the distribution of total number of infected individuals during an epidemic outbreak in the limit of large, fixed-sized populations. Our results relied upon the observation that for such populations, the probability of extreme outbreaks scaled exponentially with the population size, and was therefore describeable in terms of analytical mechanics. By analyzing the canonical SIR, SEIR, and COVID-19 models with arbitrary heterogeneity in infectivity and recovery, we were able to derive simple formulas for the paths and probabilities of extreme outbreaks. Moreover, we showed that the effective dynamics of such outbreaks due to noise entailed a constant boost (or depletion) of susceptibles and a constant increase (or decrease) in the effective recovery rate compared to the mean-field dynamics. Our approach captured the full quantitative structure of extreme outbreak probabilities: first decreasing for small outbreaks to a unique least-likely small outbreak, then increasing to a local maximum given by the mean-field theory, before decaying monotonically toward a completely infected population. Finally we showed that, unlike other well-known examples of rare events in population models, such as extinction or escape from a metastable state, the statistics of extreme outbreaks depend on an infinite number of minimum-action paths that connect initial and final outbreak states, both, with non-zero probability flux. Due to this distinct phase-space topology, extreme outbreak dynamics represents a new class of rare process for discrete-state stochastic systems. As a consequence, our approach does not require accuracy along timescales that are exponentially long in the population size (as in metastable systems), but rather logarithmic only[38].

JH and IBS were supported by the U.S. Naval Re-

search Laboratory funding (N0001419WX00055), the Office of Naval Research (N0001419WX01166) and (N0001419WX01322), and the Naval Innovative Science and Engineering award. MA was supported by the Israel Science Foundation Grant No. 531/20, and by the Humboldt Research Fellowship for Experienced Researchers of the Alexander von Humboldt Foundation.

Appendix (Supplementary Material)

First, let us list the possible reactions in the heterogeneous COVID-19 model described in the main text:

$$(S, E) \rightarrow (S-1, E+1) \text{ with rate } S \sum_n \beta_n I_n / N, \quad (\text{A1})$$

$$(E, I_n) \rightarrow (E-1, I_n+1) \text{ with rate } z_n \alpha E, \quad (\text{A2})$$

$$(I_n, R) \rightarrow (I_n-1, R+1) \text{ with rate } \gamma_n I_n. \quad (\text{A3})$$

From these, the Hamiltonian Eq.(9) directly follows.

In order to complete the description of extreme outbreaks, we need to know $x_s^*(m, C(m))$. One useful strategy for doing this is to find relationships between the time-integrals of x_e and $x_{i,n}$ and x_s . As in the main text, let us start with three of Hamilton's equations determined from Eq.(9):

$$\dot{x}_s = -x_s \left(\frac{m}{m_s} \right) \sum_n \beta_n x_{i,n}, \quad (\text{A4})$$

$$\dot{x}_{i,n} = \alpha x_e z_n \left(\frac{m_{i,n}}{m} \right) - (\gamma_n / m_{i,n}) x_{i,n}, \quad (\text{A5})$$

$$\dot{x}_r = \sum_n (\gamma_n / m_{i,n}) x_{i,n}. \quad (\text{A6})$$

By defining $I_e \equiv \int_0^\infty x_e(t) dt$ and $I_{i,n} \equiv \int_0^\infty x_{i,n}(t) dt$, we can integrate Eqs.(A5-A6) with respect to t . Remembering that $x_{i,n}(t=0) \approx 0$, $x_{i,n}(t \rightarrow \infty) \rightarrow 0$, and $x_r(t \rightarrow \infty) \rightarrow 1 - x_s^*$, the result is:

$$0 = \alpha I_e z_n \left(\frac{m_{i,n}}{m} \right) - (\gamma_n / m_{i,n}) I_{i,n} \quad (\text{A7})$$

$$1 - x_s^* = \sum_n (\gamma_n / m_{i,n}) I_{i,n}. \quad (\text{A8})$$

Similarly, separating t and x_s in Eq.(A4) and integrating over all time we get

$$\int_1^{x_s^*} \frac{m_s(x_s) dx_s}{x_s m} = - \sum_n \beta_n I_{i,n}. \quad (\text{A9})$$

Finally, if we insert $m_s = mx_s / [x_s + C(m)]$ from the main text into Eq.(A9), we can solve Eqs.(A7-A9) for $x_s^*(m, C(m))$:

$$\frac{-\ln \left\{ \frac{x_s^* + C(m)}{1 + C(m)} \right\}}{1 - x_s^*} = \sum_n \frac{z_n \beta_n m_{i,n}^2 (C(m))}{m \gamma_n}. \quad (\text{A10})$$

Altogether then, the action is expressed as a function of the constant momentum m

$$\begin{aligned} \mathcal{S}(m, x_s^*(m, C(m))) &= x_s^* \ln \left\{ \frac{m x_s^*}{C(m) + x_s^*} \right\} \\ &- \ln \left\{ \frac{m}{C(m) + 1} \right\} + C(m) \ln \left\{ \frac{C(m) + 1}{C(m) + x_s^*} \right\} \end{aligned} \quad (\text{A11})$$

All parameters in Eq.(A11) depend on m : $C(m)$ through Eq.(10) and $x_s^*(m, C(m))$ through Eq.(A10).

-
- [1] M. J. Keeling and P. Rohani, *Modeling Infectious Diseases in Humans and Animals* (Princeton University Press, 2008).
- [2] H. Andersson and T. Britton, *Stochastic epidemic models and their statistical analysis* (Springer-Verlag, New York, 2000).
- [3] R. Pastor-Satorras, C. Castellano, P. Van Mieghem, and A. Vespignani, *Rev. Mod. Phys.* **87**, 925 (2015).
- [4] H. S. Rodrigues, "Application of sir epidemiological model: new trends," (2016), arXiv:1611.02565 [physics.soc-ph].
- [5] L. Billings, W. M. Spears, and I. B. Schwartz, *Physics Letters A* **297**, 261 (2002).
- [6] S. N. Dorogovtsev, A. V. Goltsev, and J. F. F. Mendes, *Rev. Mod. Phys.* **80**, 1275 (2008).
- [7] J. Hindes and M. Assaf, *Physical review letters* **123**, 068301 (2019).
- [8] A. Volkening, D. F. Linder, M. A. Porter, and G. A. Rempala, *SIAM Review* **62**, 837 (2020), <https://doi.org/10.1137/19M1306658>.
- [9] R. C. Reiner and *et al.*, *Nature Medicine* **27**, 94 (2021).
- [10] E. L. Ray and *et al.*, medRxiv (2020), 10.1101/2020.08.19.20177493.
- [11] A. Vazquez, *Phys. Rev. E* **103**, L030301 (2021).
- [12] A. Catching, S. Capponi, M. T. Yeh, S. Bianco, and R. Andino, medRxiv (2021), 10.1101/2020.08.12.20173047.
- [13] F. Brauer, *Infectious Disease Modelling* **2**, 113 (2017).
- [14] T. Ganyani, C. Faes, and N. Hens, *Annual Review of Statistics and Its Application* **8**, 69 (2021), <https://doi.org/10.1146/annurev-statistics-061120-034438>.
- [15] C. M. Batistela, D. P. F. Correa, Á. M. Bueno, and J. C. Piqueira, *Chaos, solitons, and fractals* **142**, 110388 (2021).
- [16] J. C. Miller, "Distribution of outbreak sizes for sir disease in finite populations," (2019), arXiv:1907.05138 [q-bio.PE].
- [17] L. J. S. Allen, *Infectious Disease Modelling* **2**, 128 (2017).
- [18] T. House, J. V. Ross, and D. Sirl, *Proceedings of the Royal Society A: Mathematical, Physical and Engineering Sciences* **469**, 20120436 (2013).
- [19] F. Ball, *Advances in Applied Probability* **18**, 289 (1986).
- [20] F. Ball and D. Clancy, *Advances in Applied Probability* **25**, 721 (1993).
- [21] E. Ben-Naim and P. L. Krapivsky, *Phys. Rev. E* **69**,

- 050901 (2004).
- [22] E. Ben-Naim and P. L. Krapivsky, *The European Physical Journal B* **85**, 145 (2012).
- [23] S. Singh and C. R. Myers, *Phys. Rev. E* **89**, 042108 (2014).
- [24] M. Assaf and B. Meerson, *Journal of Physics A: Mathematical and Theoretical* **50**, 263001 (2017).
- [25] M. I. Dykman, E. Mori, J. Ross, and P. M. Hunt, *J. Chem. Phys.* **100**, 5735 (1994).
- [26] O. Ovaskainen and B. Meerson, *Trends Ecol. Evol.* **25**, 643 (2010).
- [27] R. Subramanian, Q. He, and M. Pascual, *Proceedings of the National Academy of Sciences* **118** (2021), 10.1073/pnas.2019716118.
- [28] C. C. Kerr and *et al.*, *medRxiv* (2020), 10.1101/2020.05.10.20097469.
- [29] I. B. Schwartz, J. H. Kaufman, K. Hu, and S. Bianco, (2020), 10.1101/2020.04.16.20068387.
- [30] M. Assaf and B. Meerson, *Phys. Rev. E.* **81**, 021116 (2010).
- [31] J. Hindes and I. B. Schwartz, *Phys. Rev. Lett.* **117**, 028302 (2016).
- [32] A. J. Black and A. J. McKane, *Journal of Statistical Mechanics: Theory and Experiment* **2011**, P12006 (2011).
- [33] B. Meerson and P. V. Sasorov, *Phys. Rev. E* **80**, 041130 (2009).
- [34] I. Näsell, *Extinction and Quasi-stationarity in the Stochastic Logistic SIS Model* (Springer, 2011).
- [35] I. B. Schwartz, E. Forgoston, S. Bianco, and L. B. Shaw, *J. R. Soc. Interface* **8**, 1699 (2011).
- [36] A. Kamenev and B. Meerson, *Phys. Rev. E* **77**, 061107 (2008).
- [37] E. Forgoston and R. O. Moore, *SIAM Review* **60**, 969 (2018), <https://doi.org/10.1137/17M1142028>.
- [38] M. Turkyilmazoglu, *Physica D: Nonlinear Phenomena* **422**, 132902 (2021).
- [39] D. T. Gillespie, A. Hellander, and L. R. Petzold, *J. Chem. Phys.* **138**, 170901 (2013).
- [40] L. D. Landau and E. M. Lifshitz, *Mechanics, Third Edition: Volume 1 (Course of Theoretical Physics)*, 3rd ed. (Butterworth-Heinemann, 1976).
- [41] T. Harko, F. S. Lobo, and M. Mak, *Applied Mathematics and Computation* **236**, 184 (2014).
- [42] A similar effect occurs in cell biology in a mRNA-protein genetic circuit, where fluctuations in the mRNA copy number can be effectively accounted for by taking a protein-only model with a modified production rate [44].
- [43] J. Hindes, S. Bianco, and I. B. Schwartz, *PLOS ONE* **16**, 1 (2021).
- [44] E. Roberts, S. Be'er, C. Bohrer, R. Sharma, and M. Assaf, *Physical Review E* **92**, 062717 (2015).